Int. J. Solids Structures Vol. 23, No. 8, pp. 1133–1143, 1987
Printed in Great Britain.

0020-7683/87 $3.00+.00

THERMOVISCOPLASTICITY BY FINITE ELEMENT: TENSILE AND COMPRESSION TEST

H. GHONEIM† and S. MATSUOKA
AT&T Bell Laboratories, Murray Hill, NJ 07974, U.S.A.

(*Received* 22 *January* 1986; *in revised form* 17 *June* 1986)

Abstract—The coupled thermoviscoplasticity equations are developed based on the rational theory of thermodynamics. The equations are implemented in a finite element program and applied to solving the adiabatic uniaxial tensile and compression tests of Inconel 100 at an elevated temperature (1000 K). Results of the uniaxial tensile test depict a uniform temperature drop of about 2 K, due to elastic dilation, followed by a temperature rise as plastic deformation takes place. Compression results show a non-uniform temperature rise throughout the loading history with a maximum at the mid-point of the compression specimen.

NOMENCLATURE

a	material parameter
$\mathbf{b}$	body force vector per unit mass
$[B]$	strain–displacement matrix
C_0	scaling constant
C_v	specific heat at constant deformations
$[C1]$	matrix
$[C2]$	conductivity matrix
D_2^I	second invariant of the inelastic rate of deformation tensor
$[D]$	elasticity matrix
$\overset{(4)}{D}$	fourth-order elasticity tensor
e	internal energy per unit mass
E	modulus of elasticity
$\mathbf{E}$	Green–Lagrange strain tensor
$\mathbf{E}^e$	elastic component of the Green–Lagrange strain tensor
$\mathbf{E}^I$	inelastic component of the Green–Lagrange strain tensor
$\mathbf{E}_1, \mathbf{E}_2$	load vectors
$[F]$	deformation gradient tensor
$[H]$	matrix
J_2	second invariant of the deviatoric stress tensor
k	thermal diffusivity
K	thermal conductivity
$[K1]$	stiffness matrix
$[K2]$	consistency matrix
n	strain sensitivity material parameter
$\mathbf{q}$	heat flux per unit area
$\mathbf{Q}$	nodal thermal convection vector
r	heat generation per unit mass
s	entropy per unit mass
$\mathbf{S}$	second Piola–Kirchhoff stress tensor
$\mathbf{S}'$	deviatoric stress of the second Piola–Kirchhoff tensor
t	time
T	temperature
T_R	reference temperature
$\mathbf{T}$	nodal temperature
$\mathbf{U}$	nodal displacement vector
$\mathbf{x}$	position vector
α	coefficient of thermal expansion
$\boldsymbol{\beta}$	coefficient of thermal expansion tensor
$\boldsymbol{\varepsilon}$	infinitesimal strain tensor
$\boldsymbol{\varepsilon}^{vp}$	viscoplastic component of the infinitesimal strain tensor
$\boldsymbol{\Phi}$	shape function vector
γ_1, γ_2	material parameters
ν	Poisson ratio
ψ	Helmholtz free energy
ρ	density in the undeformed configuration
$\boldsymbol{\sigma}$	stress tensor (infinitesimal deformation case)
τ	effective stress.

† Department of Mechanical Engineering, Rochester Institute of Technology, Rochester, NY 14623, U.S.A.

INTRODUCTION

Development and solution of the coupled thermomechanical equations have been gaining a growing interest among researchers. This has been engendered by the increasing realization that accurate solutions of the thermomechanical problems, particularly at an elevated temperature and/or higher rates of loadings, requires the simultaneous solution of the coupled balance of momenta and energy equations. Many works have been conducted in order to solve the coupled thermomechanical equations for elastic material[1–4] as well as viscous fluids especially in the area of molten flow simulation[5–8]. However, despite that most works have been devoted to the development of the thermomechanical equations in plastic and/or viscoplastic materials[9–12], little has been devoted to solving such equations. Allen[12, 13] presented a solution of the one-dimensional coupled thermomechanical problem in a viscoplastic uniaxial bar. Herein, we offer a comprehensive study of the development and solution of the thermodynamic problem of a class of viscoplastic materials. First, the thermoviscoplasticity equations are developed. Then, the corresponding finite element (FE) algorithm is implemented. Finally, numerical solutions of the tensile and compressive loading of a two-dimensional axisymmetric bar are presented.

DEVELOPMENT OF THE THERMOVISCOPLASTICITY EQUATIONS

The development of the thermoviscoplasticity equations is based on the rational theory of thermodynamics introduced by Coleman and Noll[14]. The theory requires three types of basic assumptions[15].

(1) The list of basic thermomechanical quantities which completely describes thermodynamic processes in a viscoplastic material.

(2) The fundamental equations of mechanics: the conservation of mass, balance of momenta, conservation of energy, and the second law of thermodynamics.

(3) Constitutive assumptions which describe the material response and abide by certain physical and mathematical requirements (axioms of constitutive theory) [16].

The list of the thermomechanical quantities which characterizes the state of every point of a body at every time (completely describes thermodynamic processes), in general, can be postulated as: the motion, $\mathbf{x}$, the second Piola–Kirchhoff stress, $\mathbf{S}$, the body force per unit mass, $\mathbf{b}$, the Helmholtz free energy, ψ, the specific entropy, s, and heat supply, r, the absolute temperature, T, the heat flux vector per unit area, $\mathbf{q}$, the inelastic strain tensor, $\mathbf{E}^{\mathrm{I}}$, and a set of internal state variables, $\boldsymbol{\alpha}^{(\mathrm{I})}$. All these quantities are functions of the reference position vector, $\mathbf{X}$, and the time t. It should be pointed out that the inelastic strain rate can be omitted from the list; to be recovered as an internal state variable[17, 18]. Also, the internal state variables may be ignored from the list, in which case the inelastic strain can be considered as an internal state variable[19]. However, because the internal state variables provide information on the microscopic state and on the microstructural defects[20] while the inelastic strain provides information only on the current geometry, it is advisable to include both quantities in the aforementioned list. Herein, the internal state variables are ignored, which restricts our analysis to perfectly viscoplastic materials and to monotonic loading conditions where both the drag and rest stresses[21] do not play a significant role.

The fundamental equations of mechanics (the balance of linear momentum, conservation of energy, and the second law of thermodynamics, respectively) are

$$\nabla \cdot \mathbf{S}\mathbf{F}^{T} + \rho(\mathbf{b} - \ddot{\mathbf{x}}) = 0 \tag{1}$$

$$\rho(\dot{\psi} + \dot{s}T + s\dot{T}) = \rho\dot{e} = \mathbf{S} : \dot{\mathbf{E}} - \nabla \cdot \mathbf{q} + \rho r \tag{2}$$

$$-\rho(\dot{\psi} + s\dot{T}) + \mathbf{S} : \dot{\mathbf{E}} - \mathbf{q} \cdot \frac{\nabla T}{T} \geqslant 0 \tag{3}$$

where ρ is the density in the reference configuration, e the specific internal energy, and $\mathbf{E}$ the Green–Lagrange strain tensor, $\mathbf{E} = \frac{1}{2}(\nabla\mathbf{x}^T \cdot \nabla\mathbf{x} - \mathbf{1})$. The superposed dot stands for the material time derivative. It might be worth mentioning that the continuity equation as well as the balance of angular momentum is implicity satisfied in eqns (1)–(3).

We consider that the knowledge of the current value of the elastic strain tensor, $\mathbf{E}^e$, the inelastic strain tensor, $\mathbf{E}^I$, the absolute temperature, and the temperature gradient, ∇T, suffice to completely determine the state of the body. Thus we can postulate the following constitutive relations:

$$\mathbf{S} = \mathbf{S}(\mathbf{E}^e, \mathbf{E}^I, T, \nabla T) \tag{4}$$

$$\psi = \psi(\mathbf{E}^e, \mathbf{E}^I, T, \nabla T) \tag{5}$$

$$s = s(\mathbf{E}^e, \mathbf{E}^I, T, \nabla T) \tag{6}$$

$$\mathbf{q} = \mathbf{q}(\mathbf{E}^e, \mathbf{E}^I, T, \nabla T) \tag{7}$$

$$\dot{\mathbf{E}}^I = \mathbf{g}(\mathbf{E}^e, \mathbf{E}^I, T, \nabla T). \tag{8}$$

Clearly constitutive relations (4)–(8) satisfy both the axioms of objectivity and equipresence.

The final form of the thermomechanical equations can be developed by invoking the axiom of admissibility; i.e. the compatibility of the constitutive equations, eqns (4)–(8), with the fundamental equations of mechanics, eqns (1)–(3). When adopting the separability of the strain tensor, $\mathbf{E} = \mathbf{E}^e + \mathbf{E}^I + \boldsymbol{\beta}(T - T_R)$, where $\boldsymbol{\beta}$ is the coefficient of the thermal expansion matrix and T_R the reference temperature, the requirement of inequality (3) yields:

(1) The response functions $\mathbf{S}$, ψ and s are independent of the temperature gradient, ∇T, that is

$$\begin{aligned} \mathbf{S} &= \mathbf{S}(\mathbf{E}^e, \mathbf{E}^I, T) \\ \psi &= \psi(\mathbf{E}^e, \mathbf{E}^I, T) \\ s &= s(\mathbf{E}^e, \mathbf{E}^I, T). \end{aligned} \tag{9}$$

(2) ψ determines both the stress tensor and the specific entropy through

$$\mathbf{S} = \rho \frac{\partial \psi}{\partial \mathbf{E}^e} \tag{10}$$

and

$$s = -\frac{\partial \psi}{\partial T} + \frac{\partial \psi}{\partial \mathbf{E}^e} : \boldsymbol{\beta}. \tag{11}$$

(3) ψ, $\mathbf{g}$ and $\mathbf{q}$ obey the general inequality

$$\left(\mathbf{S} - \rho \frac{\partial \psi}{\partial \mathbf{E}^I}\right) : \mathbf{g} - \mathbf{q} \cdot \frac{\nabla T}{T} \geqslant 0.$$

The above thermodynamic restrictions, eqns (9)–(11), may now be applied to eqn (2), yielding

$$\rho\left(\frac{\partial \psi}{\partial \mathbf{E}^I} - T\frac{\partial^2 \psi}{\partial T \partial \mathbf{E}^I}\right) : \mathbf{g} - T\frac{\partial \mathbf{S}}{\partial T} : \dot{\mathbf{E}}^e - \rho T \frac{\partial^2 \psi}{\partial T^2}\dot{T} + \dot{\mathbf{S}} : \boldsymbol{\beta} T = \mathbf{S} : \dot{\mathbf{E}}^I - \nabla \cdot \mathbf{q} + \rho r. \tag{12}$$

At this stage, introduction of closed forms for the constitutive relations (9), (7) and (8) is necessary for the analytical solution of any thermomechanical problem. First, we assume

$$\psi = \psi_0 + \tfrac{1}{2}\mathbf{E}^e : \overset{(4)}{D} : \mathbf{E}^e - C_v T \ln\left(\frac{T}{T_R} - 1\right) \tag{13}$$

and

$$\mathbf{q} = -K\nabla T \tag{14}$$

where ψ_0, $\overset{(4)}{D}$, C_v and K are material constants. $\overset{(4)}{D}$ stands for the fourth-order elasticity tensor, C_v is the specific heat at constant deformation, and K is the thermal conductivity. Applying eqns (13) and (14) together with eqns (10)–(12), we get

$$-K\nabla^2 T + \rho C_v \dot{T} = \mathbf{S} : \dot{\mathbf{E}}^I - (\boldsymbol{\beta} : \overset{(4)}{D} : \dot{\mathbf{E}}^e)T + \rho r \tag{15}$$

the first term on the right-hand side of eqn (15) is the energy dissipation function and the second term is the reversible portion of the mechanical energy generated. Furthermore, we assume the flow rule for eqn (8), that is

$$\dot{\mathbf{E}}^I = \lambda \mathbf{S}' \tag{16}$$

where $\mathbf{S}'$ is the deviatoric stress tensor. Upon squaring eqn (16) we get[22]

$$\dot{\mathbf{E}}^I = \left(\frac{D_2^I}{J_2}\right)^{1/2} \mathbf{S}' \tag{17}$$

where D_2^I is the second invariant of the inelastic rate of deformation tensor and J_2 is the second invariant of the deviatoric stress tensor. In general $D_2^I = F(J_2, T, \boldsymbol{\alpha}^{(1)})$ [23], however, for simplicity we take $D_2^I = C(J_2)^m$ which upon substituting in eqn (17) gives the power formula of the constitutive relation developed by Bodner and Partom

$$\dot{\mathbf{E}}^I = C_0 \left(\frac{\tau^E}{Y}\right)^n \frac{\mathbf{S}}{\tau^E} \tag{18}$$

where τ^E is the effective stress, $\tau^E = \sqrt{(3J_2)}$, n is a strain rate sensitivity constant ($n = m/2$), C_0 is a scaling factor, and Y is a constant which is equivalent to the yield stress[24]. It should be pointed out that the constitutive relation (18) does not account for the isotropic hardening, kinematic hardening, strain rate history nor temperature effect. However, extension of eqn (18) to consider these factors is straightforward[25–27].

Equations (1) and (15) are the coupled balance of momentum and energy equations, which together with the constitutive relations (18) and $\mathbf{S} = \overset{(4)}{D} : \mathbf{E}^e$ form the thermoviscoplastic governing equations. Knowing the thermomechanical boundary conditions, eventually, the thermodynamic boundary value problem can be analytically solved.

THE FINITE ELEMENT IMPLEMENTATION

The finite element solution is restricted to: the quasistatic infinitesimal deformation, with no body force and internal heat generation, two-dimensional problems, and isotropic materials. Consequently eqns (1) and (15) become

$$\nabla \cdot \boldsymbol{\sigma} = 0 \tag{19}$$

$$-K\nabla^2 T+\rho C_v \dot{T} = \boldsymbol{\sigma}\cdot\dot{\boldsymbol{\varepsilon}}^{vp} - a\dot{\varepsilon}_v T \tag{20}$$

where

$$\boldsymbol{\sigma} = [D]\{\boldsymbol{\varepsilon}-\boldsymbol{\varepsilon}^{vp}-\alpha(T-T_R)\boldsymbol{\delta}\} \tag{21}$$

and, from eqn (18)

$$\dot{\boldsymbol{\varepsilon}}^{vp} = C_0\left(\frac{\tau^E}{Y}\right)^n \frac{\boldsymbol{\sigma}'}{\tau^E} \tag{22}$$

where $\boldsymbol{\sigma}$ and $\boldsymbol{\varepsilon}$ are the stress and strain tensors, respectively, expressed in vector forms. $\boldsymbol{\sigma}'$ and $\boldsymbol{\varepsilon}^{vp}$ are the corresponding deviatoric stress and viscoplastic (inelastic) strain vector, respectively. $a = E/(1-2\nu)$, where E and ν are the modulus of elasticity and Poisson ratio, respectively. ε_v is the dilatation, $[D]$ the elastic matrix, and α the coefficient of thermal expansion. $\boldsymbol{\delta}$ is a vector given by $\boldsymbol{\delta}^T = (1\ 1\ 1\ 0)$ where the '0' element corresponds to the shear component and the superscript T stands for the transpose.

The spacial solution of the thermocoupled equations, eqns (19) and (20), is accomplished via the Galerkin finite element method[28]. Having expanded the displacement vector, **u**, and the temperature in terms of the shape functions, $\boldsymbol{\Phi}(r,z)$, the nodal displacement, **U**, and temperature, **T**, vectors, respectively; we enforce Galerkin conditions on eqns (19) and (20) using eqns (21) and (22) to get

$$[K1]\dot{\mathbf{U}}-[C1]\dot{\mathbf{T}} = \mathbf{R}+\mathbf{E}_1 \tag{23}$$

and

$$[C2]\dot{\mathbf{T}}+[K2]\mathbf{T} = \mathbf{Q}+\mathbf{E}_2 \tag{24}$$

where

$$\begin{aligned}
[K1] &= \int_\Omega [B]^T[D][B]\,d\Omega \\
[C2] &= \int_\Omega [\nabla\Phi][\nabla\Phi]^T\,d\Omega \\
[C1] &= \gamma_1\int [B]^T[\Phi']\,d\Omega \\
[K2] &= \frac{1}{k}\int [\Phi][\Phi]^T\,d\Omega \\
\mathbf{E}_1 &= \lambda\int [B]^T[D]\boldsymbol{\sigma}'\,d\Omega
\end{aligned} \tag{25}$$

and

$$\mathbf{E}_2 = \frac{1}{k}\int \boldsymbol{\Phi}(\boldsymbol{\sigma}\cdot\dot{\boldsymbol{\varepsilon}}^{vp})\,d\Omega - \gamma_2\left(\int [\Phi]^T\dot{\varepsilon}_v[\Phi]\,d\Omega\right)\mathbf{T}$$

where $[K1]$, $[C2]$, and $[K2]$ are the stiffness, conductivity and consistency matrices respectively. **R** and **Q** are the nodal force and the thermal convection load vectors, respectively. $\mathbf{E}_1$ is a vector which accounts for the viscoplastic effect on the momentum equation, while $\mathbf{E}_2$ accounts for the mechanical heat generation (both the reversible and irreversible parts). In eqns (25), $[B]$ is the strain–displacement matrix[29], k is the diffusivity, $\gamma_1 = a\alpha$ and

$\gamma_2 = a/K$. It is understood that eqns (23)–(25) are constructed via the standard assembly method.

Adopting the step-by-step strategy together with the 'θ' method[28] for the time marching solution of eqns (23) and (24) we get

$$[K1](\mathbf{U}^{j+1}-\mathbf{U}^{j})-[C1](\mathbf{T}^{j+1}-\mathbf{T}^{j}) = \Delta t R^{j+1}+\Delta t \mathbf{E}_1^0 \tag{26}$$

and

$$[A]\mathbf{T}^{j+1} = [H]\mathbf{T}^{j}+\Delta t Q^{j+1}+\Delta t \mathbf{E}_2^0 \tag{27}$$

where

$$[A] = [C2]+\Delta t\theta[K2]$$
$$[H] = [C2]-\Delta t(1-\theta)[K2]$$

and

$$\mathbf{E}_i^0 = \theta \mathbf{E}_i^{j+1}+(1-\theta)\mathbf{E}_i^{j} \quad \text{for} \quad i = 1,2.$$

Equations (26) and (27) can be rearranged as

$$[K1]\mathbf{U}^{j+1} = \mathbf{N}_1 \quad \text{and} \quad [A]\mathbf{T}^{j+1} = \mathbf{N}_2 \tag{28}$$

where all the nonlinearity is contained in the vectors $\mathbf{N}_1$ and $\mathbf{N}_2$. Consequently at each time step $[K1]$ and $[A]$ are constructed and decomposed, using the LU decomposition method, only once. This simple method (the initial load method) turns out to be very efficient for the class of problems handled herein, particularly when the successive iteration involved in eqns (28) for the solution of $\mathbf{U}^{j+1}$ and $\mathbf{T}^{j+1}$ at each time step is improved via the Aitken acceleration method[30].

NUMERICAL RESULTS AND DISCUSSIONS

Two examples are studied: (1) adiabatic uniaxial tensile loading, (2) adiabatic compressive loading of a cylindrical bar with constraint ends (constrained from lateral motions). A fixed temperature boundary condition is assumed at the constraint ends. For small deformation and massive cross heads, the constraint ends and fixed temperature boundary conditions are reasonable. Both numerical tests are conducted for Inconel 100 (IN100) at 1000 K ambient temperature. At such an elevated temperature IN100 is known to behave viscoplastically[31] and can be well approximated by Bodner and Parton's constitutive equations[32]. The following material constants are considered:

$$E = 173 \text{ GPa } (25.1\times10^6 \text{ psi})$$
$$Y = 860 \text{ MPa } (125\times10^3 \text{ psi})$$
$$\nu = 0.284, \quad n = 20, \quad C_0 = 0.0001 \text{ s}^{-1}$$
$$\rho = 9500 \text{ kg m}^{-3} \ (0.343 \text{ lb in}^{-3})$$
$$C_v = 525 \text{ J kg}^{-1} \text{ K}^{-1} \ (0.125 \text{ Btu lb}^{-1} \text{ °F}^{-1})$$
$$K = 21.7 \text{ W m}^{-1} \text{ K}^{-1} \ (151 \text{ Btu ft}^{-2} \text{ in}^{-1} \text{ h}^{-1} \text{ °F}^{-1})$$

and

$$\alpha = 14.4\times10^{-6} \text{ K}^{-1} \ (8.3\times10^{-6} \text{ °F}^{-1}).$$

Except for C_0 and n which are determined by numerical exercises, all the above material constants are obtained from Ref. [33].

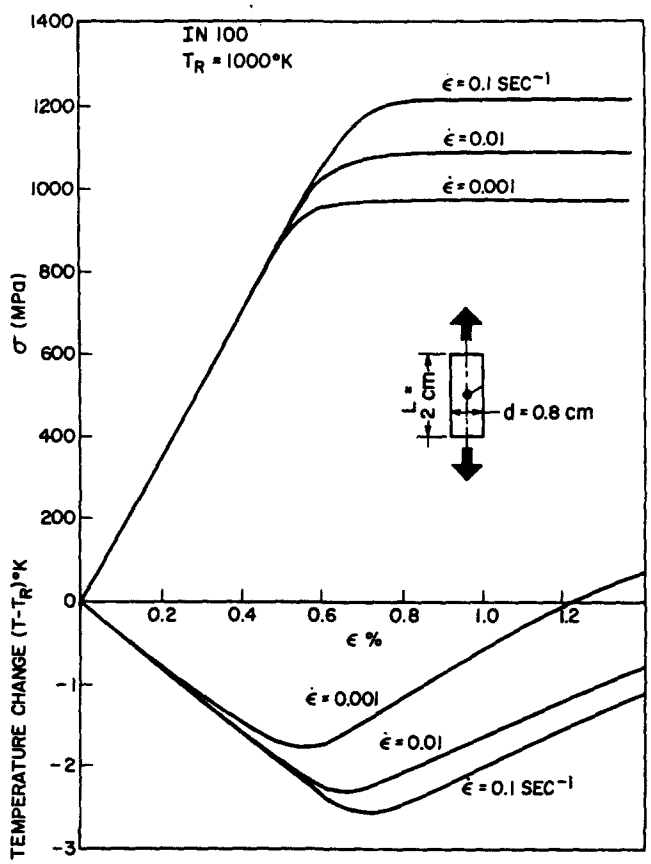

Fig. 1. The predicted stress and temperature change of the uniaxial test at different strain rates.

Since the uniaxial tensile loading is a one-dimensional problem with the temperature and the stress uniform throughout most of the tensile specimen, two elements are used to simulate the tensile testing and to find the uniform temperature and stress. Figure 1 shows the stress–strain results at different strain rates together with the corresponding temperature change. The figure demonstrates the strain rate sensitivity of the IN100, and depicts the temperature drop during tensile elastic loading which is followed by a temperature rise as the plastic deformation takes place. This temperature change is in accordance with the entropy concept and has its experimental supportive evidences[34].

Figure 2 displays the engineering stress–strain results, for the compression test, and the corresponding temperature change at three different points along the center line of the specimen. In general, unlike the tensile loading, the temperature rises throughout the loading history during elastic deformation as a result of local contractions, and during plastic deformation due to the energy dissipation. At the vicinity of the constraint ends, results depict that at a higher level of loading ($\varepsilon \geqslant 0.6\%$) when bulging starts to take place, elastic dilatation is experienced which explains the temperature drop at point 3 (Fig. 2). Figures 3(a)–(d) display the contour plots of the effective stress and temperature change at different stages of loadings: $\varepsilon = 0.3$, 0.6, 0.9, and 1.2%, respectively. (Contour lines 1, 2, 3,... are 300, 350, 400,... MPa for the stress and 0.0, 0.5, 1.0, 1.5 K,... for the temperature, respectively.) Note that because of symmetry, only one quarter of the specimen is considered (the upper right-hand side portion). Contour plots show that, in general, the effective stress is higher at both the corners and the midpoint with the minimum values in the vicinity of the center line of the constraint ends. It might be worth mentioning that since the effective stress is the criterion of plastic deformation, the contour plots of the effective stress represent the plastic zone propagation: initiates at the corners and the midpoint then spreads diagonally[24]. This agrees with the numerical results in Ref. [35]. The temperature contour plots (Fig. 3) show that, in general, the temperature rise is maximum at the midpoint and

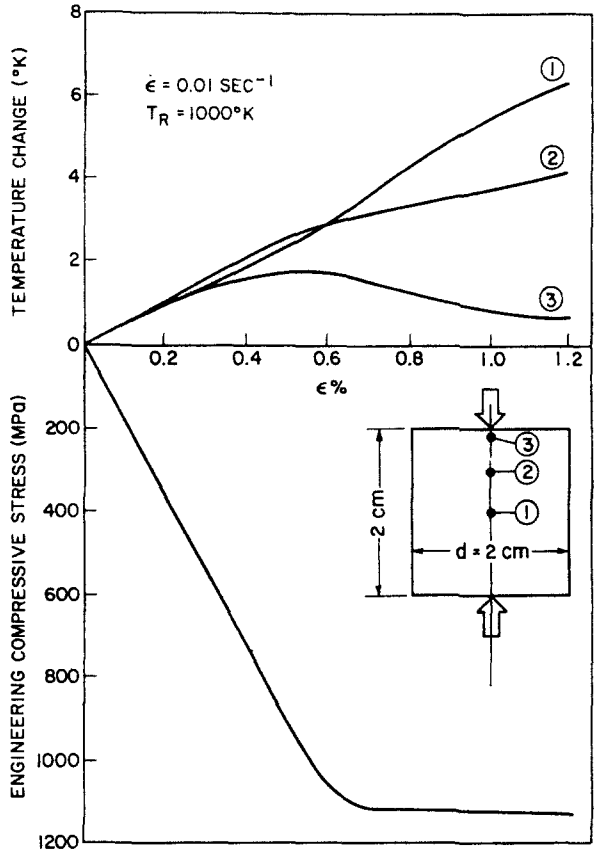

Fig. 2. The predicted engineering stress and temperature changes of the compression test.

decreases gradually in the radial direction and along the center line as we move toward the constraint ends, with the highest temperature gradient near the constraint ends. It might be noticed that the calculated temperature change due to the elastic dilation effect, in general, is small (0.3%) which suggests that the coupled equations are more useful for the cases where accurate prediction of the temperature and/or temperature gradient are

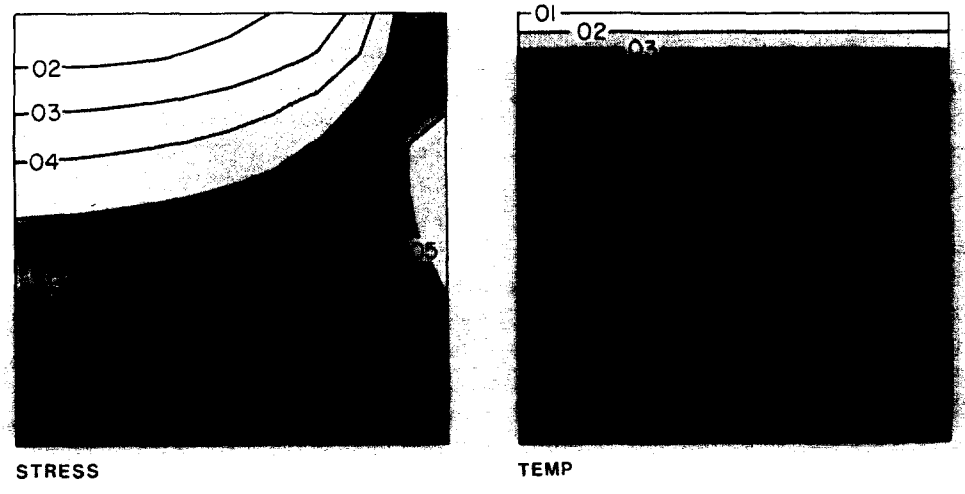

(a)

Fig. 3. The predicted effective stress and temperature change fields of the compression test at different stages of loadings.

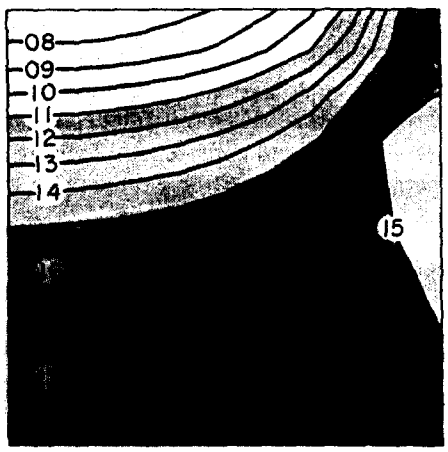

STRESS

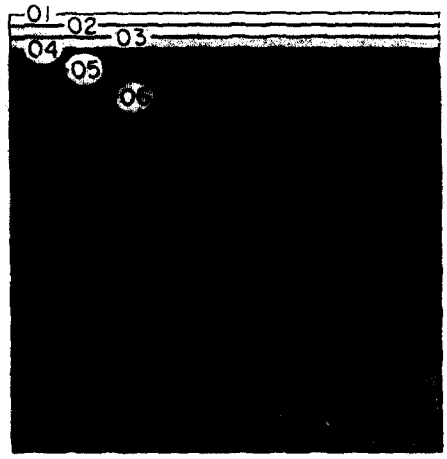

TEMP

(b)

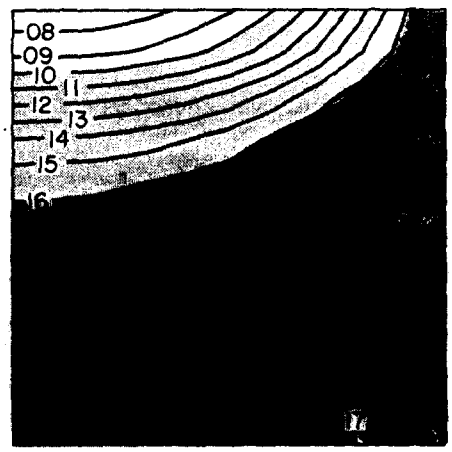

STRESS

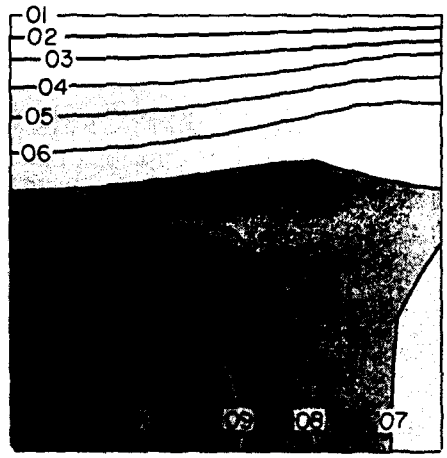

TEMP

(c)

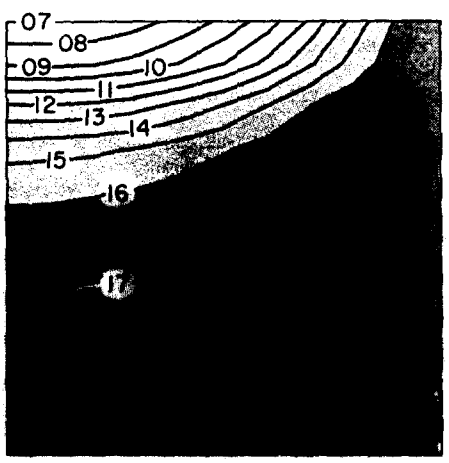

STRESS

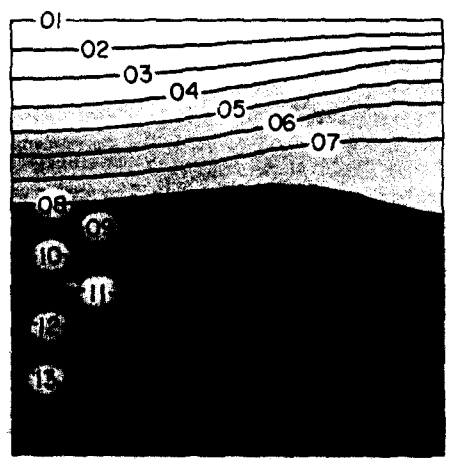

TEMP

(d)

important as well as for the cases where extremely high strain rates or finite strain are considered.

It should be pointed out that unless eqn (22) is modified to account for the work hardening, cyclic loading will not be properly simulated by the current analysis. Consequently no attempts have been made to analyze cyclic loading. This together with the experimental verifications will be investigated in future works. However, one can foresee that cyclic loading at the same conditions as those of tensile and compression loading will generate a considerable amount of heat and temperature rise.

CONCLUSION

Accurate solution of the thermoviscoplasticity problems requires the solution of the coupled balance of momenta and energy equations. Numerical solution of the thermoviscoplasticity problem of tensile loading of IN100 at 1000 K predicted a uniform temperature drop of about 2 K, due to elastic dilation, followed by a temperature rise as the plastic deformation occurs. A compression test predicted a non-uniform temperature rise, throughout the loading history, with a maximum at the mid-point of the compression specimen. Results, in general, show that at an elevated temperature and higher rates of loading of viscoplastic materials a noticeable amount of heat and temperature rise can be generated.

REFERENCES

1. C. V. Massalas and V. K. Kalpakidis, Coupled thermoelastic vibration of a Timoshinko beam. *Lett. Appl. Engng Sci.* **22**, 459–465 (1984).
2. Y. Y. Li, H. Ghoneim, Y. Chen and J. Davis, A numerical method in solving a coupled thermoelasticity equation and some results. *J. Thermal Stresses* **6**, 253–280 (1983).
3. L. Bahar and R. B. Hetnarski, Coupled thermoelasticity of a layered medium. *J. Thermal Stresses* **3**, 141–152 (1980).
4. M. Berkovic, On the nonlinear transient analysis of the coupled thermomechanical phenomena. *Comput. Struct.* **10**, 195–202 (1979).
5. H. Ghoneim and S. Matsuoka, Simulation of balancing multi-cavity molds. Tech. Memo., Bell Laboratories, Murray Hill, New Jersey (1983).
6. J. M. Custro, On the mathematical modeling of the reaction injection molding (RIM) process. *Latin Am. J. Chem. Engng Appl. Chem.* **6**, 67–87 (1982).
7. C. Douglas and D. Roylance, Finite element analysis of nonisothermal polymer processing operations. MIT Department of Materials Science and Engineering, Research Report No. R82-1 (1982).
8. C. A. Hieber and S. F. Shen, A finite element/finite difference simulation of the injection molding filling process. *J. Non-Newtonian Fluid Mech.* 7, 1–32 (1980).
9. M. B. Rubin, A thermoelastic–viscoplastic model with a rate-dependent yield strength. *J. Appl. Mech. ASME* **49**, 305–311 (1982).
10. P. Perzyna, Coupling of dissipative mechanisms of viscoplastic flow. *Arch. Mech.* **29**, 607–624 (1977).
11. J. Kratochvil and O. W. Dillon, Thermodynamics of crystalline elastic–visco-plastic materials. *J. Appl. Phys.* **11**, 1470–1479 (1970).
12. D. H. Allen, Predicted axial temperature gradient in a viscoplastic uniaxial bar due to thermomechanical coupling. *Int. J. Numer. Meth. Engng* **23**, 903–917 (1986).
13. D. H. Allen, A prediction of heat generation in a thermoviscoplasticity uniaxial bar. *Int. J. Solids Structures* **21**, 325–343 (1985).
14. B. D. Coleman and W. Noll, The thermodynamics of elastic materials with heat conduction and viscosity. *Archs Ration. Mech. Analysis* **13**, 167 (1963).
15. J. Kratochvil and O. W. Dillon, Thermodynamics of elastic–plastic materials as a theory with internal state variables. *J. Appl. Phys.* **40**, 3207–3218 (1967).
16. A. C. Eringen, *Mechanics of Continua*. Wiley, New York (1967).
17. D. H. Allen, Thermodynamic constraints on the constitution of a class of thermoviscoplastic solids. Texas A&M University Mechanics and Materials Center, Report No. MM12415-82-10 (1982).
18. K. C. Valanis, A theory of viscoplasticity without a yield surface. *Arch. Mech.* **23**(4), 517–551 (1971).
19. P. Perzyna and W. Wojno, Thermodynamics of rate sensitive plastic material. *Arch. Mech.* **20**, 499 (1968).
20. B. D. Coleman and M. E. Grutin, Thermodynamics with internal state variables. *J. Chem. Phys.* **47**, 597–613 (1967).
21. A. K. Miller, Modeling of cyclic plasticity with unified constitutive equations: improvement in simulation normal and anomalous Bauschinger effects. *J. Engng Mater. ASME* **102**, 215–222 (1980).
22. S. R. Bodner and Y. Partom, A large deformation elastic–viscoplastic analysis of a thick-walled spherical shell. *J. Appl. Mech. ASME* **39**, 751–757 (1972).
23. S. R. Bodner, I. Partom and Y. Partom, Uniaxial cyclic loading of elastic viscoplastic materials. *J. Appl. Mech. ASME* **46**, 805–810 (1979).
24. H. Ghoneim and Y. Chen, A viscoelastic–viscoplastic constitutive equation and its finite element implementation. *Comput. Struct.* **17**(4), 499–509 (1983).

25. S. R. Bodner and Y. Partom, Constitutive equations for elastic–viscoplastic strain hardening materials. *J. Appl. Mech.* **42**, 385–389 (1975).
26. S. R. Bodner and A. Merzer, Viscoplastic constitutive equations for copper with strain rate history and temperature effects. *J. Engng Mater. Tech. ASME* **100**, 388–394 (1978).
27. H. Ghoneim, S. Matsuoka and Y. Chen, Viscoplastic modeling with strain rate history dependency. *J. Appl. Mech. ASME* **50**, 465–468 (1983).
28. J. N. Reddy, *An Introduction to Finite Element Method.* McGraw-Hill, New York (1984).
29. J. A. Zienkiewicz, *The Finite Element Method*, 3rd Edn. McGraw-Hill, London (1977).
30. Y. K. Chow and S. Kay, On the Aitken acceleration method for nonlinear problems. *Comput. Struct.* **19**, 757–761 (1984).
31. D. C. Stouffer, A constitutive representation for IN100. Air Force Material Laboratories, AFWAL-TR-81-4039 (1981).
32. T. M. Milly and D. H. Allen, A comparative study of nonlinear rate dependent mechanical constitutive theory for crystalline solids at elevated temperatures. Virginia Polytechnic Institute and State University, VPI-E-82-5 (1982).
33. *High Temperature High Strength Nickel Base Alloys*, 3rd Edn. The International Nickel Company Inc. (1977).
34. S. Matsuoka and H. E. Bair, The temperature drop in glassy polymers during deformation. *J. Appl. Phys.* **48**(10), 4058–4062 (1977).
35. C. Bohatier and J. Chento, Finite element formulations for non-steady-state large viscoplastic deformations. *Int. J. Numer. Meth. Engng* **21**, 1697–1708 (1985).